

RESEARCH ARTICLE | DECEMBER 07 2023

On the description of conical intersections between excited electronic states with LR-TDDFT and ADC(2)

Jack T. Taylor ; David J. Tozer ; Basile F. E. Curchod  



J. Chem. Phys. 159, 214115 (2023)

<https://doi.org/10.1063/5.0176140>

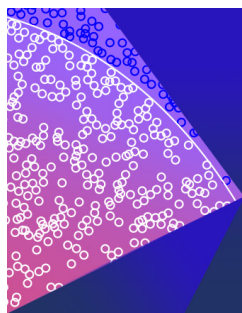


View
Online



Export
Citation

CrossMark



The Journal of Chemical Physics

Special Topic: Monte Carlo methods,
70 years after Metropolis *et al.* (1953)

Submit Today

On the description of conical intersections between excited electronic states with LR-TDDFT and ADC(2)

Cite as: J. Chem. Phys. 159, 214115 (2023); doi: 10.1063/5.0176140

Submitted: 11 September 2023 • Accepted: 14 November 2023 •

Published Online: 7 December 2023



View Online



Export Citation



CrossMark

Jack T. Taylor,¹  David J. Tozer,^{1,a)}  and Basile F. E. Curchod^{2,b)} 

AFFILIATIONS

¹Department of Chemistry, Durham University, South Road, Durham DH1 3LE, United Kingdom

²Centre for Computational Chemistry, School of Chemistry, University of Bristol, Cantock's Close, Bristol BS8 1TS, United Kingdom

^{a)}Electronic mail: d.j.tozer@durham.ac.uk

^{b)}Author to whom correspondence should be addressed: basile.curchod@bristol.ac.uk

ABSTRACT

Conical intersections constitute the conceptual bedrock of our working understanding of ultrafast, nonadiabatic processes within photochemistry (and photophysics). Accurate calculation of potential energy surfaces within the vicinity of conical intersections, however, still poses a serious challenge to many popular electronic structure methods. Multiple works have reported on the deficiency of methods like linear-response time-dependent density functional theory within the adiabatic approximation (AA LR-TDDFT) or algebraic diagrammatic construction to second-order [ADC(2)]—approaches often used in excited-state molecular dynamics simulations—to describe conical intersections between the ground and excited electronic states. In the present study, we focus our attention on conical intersections *between excited electronic states* and probe the ability of AA LR-TDDFT and ADC(2) to describe their topology and topography, using protonated formaldimine and pyrazine as two exemplar molecules. We also take the opportunity to revisit the performance of these methods in describing conical intersections involving the ground electronic state in protonated formaldimine—highlighting in particular how the *intersection ring* exhibited by AA LR-TDDFT can be perceived either as a (near-to-linear) seam of intersection or two interpenetrating cones, depending on the magnitude of molecular distortions within the branching space.

© 2023 Author(s). All article content, except where otherwise noted, is licensed under a Creative Commons Attribution (CC BY) license (<http://creativecommons.org/licenses/by/4.0/>). <https://doi.org/10.1063/5.0176140>

I. INTRODUCTION

A theoretical understanding of almost all chemical processes arguably stems from the fundamental concept of static potential energy surfaces (PESs), a consequence of invoking the Born–Huang representation¹ for the molecular wavefunction. Of particular significance to photochemical (and photophysical) processes is the notion of conical intersections (CXs), which correspond to molecular geometries where two (or more) adiabatic PESs become energetically degenerate.^{2–4} In contrast to initial opinions,^{5,6} it is now agreed⁷ that CXs are far from arcane mathematical curiosities. Instead, they play a critical mechanistic role in our theoretical framework to understand the ultrafast, nonradiative decay from the excited electronic states of a molecule to its ground electronic state.^{8–11} Uncovering the pivotal influence of CXs within photochemistry has triggered a plethora of works, both from an applied and theoretical perspective.^{12–18}

Formally, CXs only appear when using an adiabatic electronic basis (i.e., the eigenstates of the electronic Hamiltonian) within the Born–Huang representation¹ of the molecular wavefunction.¹⁹ A CX between two states comprises an $(F - 2)$ -dimensional seam (or intersection) space (where $F = 3N - 6$ nuclear degrees of freedom for a nonlinear molecule with N atoms) and an orthogonal two-dimensional branching¹⁵ (or $g - h$)²⁰ space. The branching space is spanned by two vectors that depend on the nuclear coordinates, \mathbf{R} : the gradient difference vector, $\mathbf{g}_{ij}(\mathbf{R})$, and the derivative coupling vector, $\mathbf{h}_{ij}(\mathbf{R})$, where i and j denote electronic states. Movement along these two vectors lifts the energy degeneracy, doing so linearly, giving the characteristic double-cone topology within the branching space.²¹ The intersection point that appears when plotting the double cone is the $(F - 2)$ -dimensional seam space, so there remain $F - 2$ nuclear degrees of freedom within the seam space for which the two PESs have the same energy. Moreover, the local minima within the seam space—termed minimum-energy CXs (MECXs)—are

typically used to characterize the nonadiabatic transitions between the electronic states.²²

As always, the insolubility of the exact electronic Schrödinger equation for chemically relevant systems necessitates using approximate electronic structure methods. Whether a given electronic structure method can adequately predict the *topology* (i.e., the dimensionality of the CX branching or seam spaces) and the *topography* (i.e., the shape of the PESs in the vicinity of the CX point within the branching space) of a given CX is a key consideration in nonadiabatic molecular dynamics simulations.²³ Much attention has therefore been paid to benchmarking different electronic structure methods in this context—see Ref. 24 for a recent review. Two requirements are often highlighted as being critical for an accurate description of CXs involving the ground electronic state: (i) inclusion of dynamic and static electron correlation, given that the character of the electronic states changes rapidly in the vicinity of (and passing through) a CX; (ii) a balanced treatment of the ground and excited electronic states, so as to allow explicit coupling between them.^{23,25} The obvious electronic structure methods of choice have thus been multiconfigurational and multireference methods^{23,26–31} such as multiconfigurational self-consistent field (MCSCF) and multireference configuration interaction (MRCI) with the state-averaged complete active space self-consistent field (SA-CASSCF)³² approach being the most widely used. A popular alternative that extends upon SA-CASSCF by including a more balanced description of dynamic correlation, which has seen a recent rise in use within excited-state molecular dynamics simulations,^{28,33–39} is extended multistate complete active space second-order perturbation theory (XMS-CASPT2).^{26,40–43}

Given the high computational cost of multiconfigurational and multireference methods and the ever-increasing size of the systems to which they need to be applied, cheaper alternatives to add to the photochemists' toolkit are still in demand. Using simpler, single-determinant methods—often designed for calculations of excited electronic states within the Franck–Condon (FC) region—to describe CXs between the *ground* and *excited electronic states* has, however, proven problematic. Notable examples include linear-response time-dependent density functional theory within the adiabatic approximation (AA LR-TDDFT),^{44–47} algebraic diagrammatic construction (ADC) methods,^{48–51} and coupled cluster theories.^{52–58} In particular, AA LR-TDDFT [within the Tamm–Dancoff approximation (TDA)⁵⁹] and ADC(2) have been thoroughly tested due to the appeal of using these low-cost electronic structure methods within nonadiabatic molecular dynamic simulations.^{60–64}

In contrast, little is known⁶⁵ about the precise quality of these cheaper approaches in describing CXs *between excited electronic states*. Although considering electronic energies alone may suggest an adequate representation of CXs within AA LR-TDDFT/TDA and ADC(2) in this context, is this what one observes in practice? How well do the topology and topography of CXs between excited electronic states given by these single-determinant methods reproduce those predicted by multiconfigurational and multireference techniques?

The present study attempts to address these questions from a pragmatic perspective by investigating the ability of AA LR-TDDFT/TDA and ADC(2) to describe CXs between the lowest two excited singlet electronic states, S_1 and S_2 , for two exemplar

molecules, protonated formalimine and pyrazine. We also revisit the problem faced by AA LR-TDDFT/TDA in describing CXs between the ground electronic state, S_0 , and S_1 for the case of protonated formalimine, focusing on the behavior of the PESs within the branching space at varied distances away from the MECX geometry. Despite providing a static, electronic structure perspective in this work, we bear nonadiabatic molecular dynamics in mind, choosing to compare our AA LR-TDDFT/TDA and ADC(2) results to reference XMS-CASPT2 results. Our work is organized as follows: We start by (i) reviewing the problem of CXs involving the ground electronic state from AA LR-TDDFT and considering issues relevant to CXs between excited states, before (ii) presenting the computational details of our calculations. We then (iii) explore the S_2/S_1 and S_1/S_0 MECX branching spaces of protonated formalimine as predicted by the three electronic structure methods, followed by (iv) the S_2/S_1 MECX of pyrazine, where further considerations of the exchange–correlation functional used in AA LR-TDDFT/TDA are provided.

II. METHODS

A. Notes on the description of conical intersections with AA LR-TDDFT

The inaccurate description of PESs in the vicinity of CXs involving the ground electronic state is, by now, a well-reported deficiency of LR-TDDFT within the AA. The first investigation to highlight this problem was that presented in the work of Levine *et al.*,⁶⁵ where for linear H_2O the dimensionality of the intersection was shown to be $F - 1$ rather than $F - 2$ (i.e., incorrect topology), while for H_3 the shape of the first excited-state PES was shown to vary too rapidly near the intersection point (i.e., incorrect topography), despite the CX possessing the correct dimensionality. The authors of the work of Tapavicza *et al.*⁶⁶ subsequently showed that applying the TDA not only helps to reduce excited-state instability problems but also gives an approximate S_1/S_0 CX for oxirane with a slightly interpenetrating double cone. Further studies have provided additional examples of the issues of AA LR-TDDFT in describing CXs between the ground and first excited electronic states, e.g., see Refs. 23 and 67–70. We note, however, that AA LR-TDDFT has been shown to predict reasonably accurate S_1/S_0 CX geometries and branching planes, despite issues with the PESs.^{65,71}

A common starting point for analyzing the deficiencies of AA LR-TDDFT is to consider the description of CXs involving the ground state within the alternative (wavefunction) approach of configuration interaction singles (CIS). Like AA LR-TDDFT, CIS (i) uses a single Slater determinant as its reference and (ii) comprises a set of linear equations restricted to a single-excitation subspace. Hamiltonian matrix elements between the Hartree–Fock (HF) ground state and singly excited Slater determinants are zero by virtue of Brillouin's theorem,⁷² meaning there is no coupling between ground and excited states in CIS. It follows that one of the two conditions for electronic degeneracy^{2,73} at a CX is satisfied trivially and the derivative coupling vector, $\mathbf{h}_{01}(\mathbf{R})$, is zero (either within just the seam space, or for any nuclear configuration, depending on how the derivative coupling vector is defined⁷³). As a result, CIS exhibits a linear ($F - 1$)-dimensional intersection [as opposed to a conical ($F - 2$)-dimensional intersection], where the

degeneracy is only lifted along one (not both) branching space vector direction(s).^{65,66} Given the CIS excited state and HF reference state do not “see each other” due to the lack of coupling,⁶⁶ their corresponding PESs cross each other within the branching space, leading to regions where the CIS excited state becomes lower in energy than the HF reference state (i.e., one observes negative excitation energies). The HF reference state struggles to reproduce the necessary rapid change in electronic character near the CX.⁶⁵

Despite the similarity between the approaches, these CIS arguments cannot be used to explain why AA LR-TDDFT fails to correctly describe CXs between the ground and excited electronic states. This is because Brillouin’s theorem does *not* hold within (LR-TD)DFT^{47,66,74} because the method does not provide formal access to wavefunctions (only electron densities). The Kohn–Sham (KS) determinant is the wavefunction of the noninteracting system, not the interacting system. Similarly, while excited-state wavefunctions can be reconstructed using excited KS determinants (for electronic state assignment purposes, see Ref. 45), they do not correspond to excited-state wavefunctions of the interacting system. The situation is reminiscent of the calculation of $\langle S^2 \rangle$ /spin contamination in DFT, whereby the usual single-determinant expression is not appropriate for the interacting system.^{75,76} In spite of the absence of Brillouin’s theorem, it is still argued^{24,77–80} that there is no coupling between the ground and excited states in AA LR-TDDFT and so the method is expected to exhibit *similar* CX problems to CIS. This lack of coupling in LR-TDDFT is a consequence of using the adiabatic approximation, as well as the ground-state exchange–correlation functional approximation. Within AA LR-TDDFT, the ground (reference) state is variationally obtained within an initial DFT calculation, separate to the singly excited (response) states, which are obtained when the Casida equation is solved [i.e., $E_j(\mathbf{R}) = E_0(\mathbf{R}) + \omega_j(\mathbf{R})$, where $\omega_j(\mathbf{R})$ is the j th vertical excitation energy].⁸⁰ The ground and excited states are therefore not treated on an equal footing, and so the coupling between them is absent. We note, this is the same reason why ADC(2) struggles to accurately predict CXs involving the ground state—the ground state is obtained at the MP2 level of theory, whereas the excited states are obtained with ADC(2).⁸¹

Many attempts have been made to fix (or, at least, circumvent) the incorrect description of CXs involving the ground electronic state within AA LR-TDDFT; these approaches can be broadly divided into two categories: (i) those that artificially expand the dimension of the LR-TDDFT/(TDA) problem to introduce coupling between the ground and excited states and (ii) those rooted solely within the formal linear-response framework of TDDFT. For the first category, methods either incorporate explicit double excitations^{78,82,83} (since these introduce coupling between the ground and excited states within a configuration interaction picture, improving upon CIS) or include direct coupling between the reference KS determinant and (at least one) singly excited determinant(s).^{79,84–86} Some fulfill this goal by using DFT quantities in a larger CI-type matrix, interpreting Slater determinants constructed from KS orbitals as approximations to the real, interacting wavefunctions,^{82–84} while others add selected excited contributions to the AA LR-TDDFT/TDA matrix equations from those derived within many-body perturbation theory.⁷⁸ The second category of methods instead comprise different variants of standard LR-TDDFT; they generate, via a modified linear-response

formalism, the ground and excited states of interest *together* as response states from a sacrificial reference state^{73,80,87,88} while still preserving the AA. These methods include spin-flip TDDFT,^{55,89,90} particle–particle RPA/(TDA),^{77,91–93} and hole–hole TDA^{94,95} and, in all cases, the resulting ground and excited states are treated on the same footing.

The aforementioned approaches are pragmatic. However, the ultimate goal within conventional LR-TDDFT is to rigorously go beyond the AA by using a frequency-dependent exchange–correlation kernel. In the exact case, the LR-TDDFT matrix problem represents a set of nonlinear equations⁹⁶ that, despite being built in a basis of single excitations, have folded in all the information from double and higher (de-)excitations thanks to the frequency dependence of the exact exchange–correlation kernel.^{78,97,98} It could be argued (i.e., along similar lines to comments made by Huix-Rottlant and Casida in Ref. 78) that a combination of these single, double, and higher (de-)excitations from the DFT reference state (i.e., a single KS determinant) could lead to the true correlated ground state being reproduced in the linear-response excitation manifold along with the (similarly correlated) excited states.^{99,100} The ground and excited electronic states would then, therefore, be treated on an equal footing, establishing the required coupling between them.

We now address a less frequently asked question: how well does AA LR-TDDFT perform for CXs between excited electronic states? Given that excited states are treated on an equal footing within LR-TDDFT (i.e., they are obtained *together* when one solves the Casida equation), it may be expected that, even in the AA, the coupling between respective excited states is indeed present. As a result, the aptitude of AA LR-TDDFT to correctly predict the topology and topography of CXs between excited electronic states is often taken for granted, even if little (in the way of explicit plotting of the excited-state CX branching spaces) is known about the performance of the method in this context.¹⁰¹ We note that the same also applies to excited electronic states obtained with ADC(2). One aspect, in particular, that requires attention when discussing CXs between excited electronic states with LR-TDDFT is the description of the branching space vectors, especially the derivative coupling vector, $\mathbf{h}_{ij}(\mathbf{R})$ [and, by extension, the closely related (first-order) nonadiabatic coupling vector, $\mathbf{d}_{ij}(\mathbf{R})$, where $\mathbf{h}_{ij}(\mathbf{R}) = [E_j(\mathbf{R}) - E_i(\mathbf{R})] \times \mathbf{d}_{ij}(\mathbf{R})$]. The $\mathbf{h}_{ij}(\mathbf{R})$ vectors between the ground and excited electronic states are well defined in linear-response TDDFT and can be derived from the excited electronic density.^{60,102–107} These $\mathbf{h}_{01}(\mathbf{R})$ vectors are formally exact within the limit that LR-TDDFT, itself, becomes exact (i.e., beyond the AA and when using the exact ground-state exchange–correlation functional), and they only become approximate when the aforementioned approximations are invoked. This contrasts with the $\mathbf{h}_{01}(\mathbf{R})$ vectors in CIS, which, as already mentioned, are formally zero by definition. On the other hand, the $\mathbf{h}_{ij}(\mathbf{R})$ vectors between excited electronic states can be defined in CIS, but their quality depends on the accuracy of the underlying CIS level of theory used to describe the coupled electronic states. The situation is different for LR-TDDFT, as even in the exact case, the $\mathbf{d}_{ij}(\mathbf{R})$ vectors [and therefore the $\mathbf{h}_{ij}(\mathbf{R})$ vectors] between excited electronic states can formally only ever be approximate within a linear-response formalism—quadratic-response is required to derive an exact expression.^{108–112} While numerical tests indicate that

$\mathbf{d}_{ij}(\mathbf{R})$ vector between excited electronic states might be fairly well approximated within a linear-response formalism,^{108,113} in particular within the TDA, a proper description of the branching space for CXs between excited electronic states is far from granted within AA LR-TDDFT, despite its routine use in excited-state dynamics simulations involving multiple excited electronic states. This work hopes to provide some reassurance on the behavior of AA LR-TDDFT/TDA [and ADC(2)] for CXs involving two excited electronic states.

B. Computational details

1. Electronic structure

All XMS-CASPT2 energies, energy gradients,¹¹⁴ and nonadiabatic coupling vectors¹¹⁵ were determined with the BAGEL 1.2.0 program package.¹¹⁶ The single-state, single-reference (SS-SR) contraction scheme^{114,117} was employed for all XMS-CASPT2 calculations with a real vertical shift of 0.3 a.u. to avoid intruder state issues. Density fitting and frozen core approximations were also applied. For protonated formaldimine, a three-state averaging and a (6/4) active space, comprising the two pairs of C–N $\sigma\sigma^*$ and $\pi\pi^*$ orbitals [Fig. S1(a)], were used (following Ref. 118). For pyrazine, a three-state averaging and a (10/8) active space, including the six π orbitals and two nitrogen lone pairs [Fig. S1(b)], were employed (based on Ref. 119). All DFT^{120–122} and AA LR-TDDFT/TDA energies, energy gradients, and nonadiabatic coupling vectors were determined with a development version of the graphics processing unit (GPU)-accelerated TeraChem 1.9 program package.^{123–129} The PBE0 (global hybrid) exchange–correlation functional^{130–132} was used throughout (unless otherwise stated—see the supplementary material) within the TDA. All MP2¹³³ and ADC(2) energies and energy gradients^{51,134} were determined with the Turbomole 7.4.1 program package,^{135,136} employing frozen core and resolution of identity¹³⁷ approximations. The Dunning cc-pVTZ basis set was used in all XMS-CASPT2, MP2, and ADC(2) calculations, whereas the Dunning cc-pVDZ basis set was used in all DFT and AA LR-TDDFT/TDA calculations.¹³⁸ The density fitting procedure, utilized in all XMS-CASPT2 calculations, made use of the cc-pVTZ-jkfit auxiliary basis set from the BAGEL library. For clarity, we will drop the “AA” hereafter when discussing our LR-TDDFT/TDA results. For quantities involving excited states only, we use the notation LR-TDDFT/TDA/PBE0 and ADC(2). For quantities involving ground and excited states, we use the notation (LR-TD)DFT/TDA/PBE0 and MP2/ADC(2).

2. Critical geometries and linear interpolation in internal coordinates

a. Protonated formaldimine. The S_0 minimum (commonly denoted FC), S_2/S_1 MECX, and S_1/S_0 MECX geometries were first optimized with XMS-CASPT2. MECX geometry optimization utilized the gradient-projection algorithm presented in the work of Bearpark *et al.*¹³⁹ Linear interpolation in internal coordinates (LIICs) pathways were generated to connect these three critical geometries of protonated formaldimine. An LIIC pathway serves as the most direct way of connecting two key points in configurational space by interpolating new points based on internal (rather than Cartesian) coordinates,¹⁴⁰ as such, they do not constitute minimum-energy pathways. A single-point XMS-CASPT2 energy calculation

was performed for each geometry to obtain the three lowest electronic states, S_0 , S_1 , and S_2 , along the LIIC. Electronic energies are given relative to the S_0 energy at the S_0 minimum.

The same procedure was repeated to acquire the electronic energies along corresponding LIIC pathways for (LR-TD)DFT/TDA/PBE0 and for MP2/ADC(2), respectively. As noted in Sec. II A, neither (LR-TD)DFT/TDA, nor MP2/ADC(2) adequately describe the branching space of S_1/S_0 CXs. Therefore, we use the term minimum-energy *crossing points* (MECPs) instead of minimum-energy *conical intersections* (MECXs) when referring to the S_1/S_0 intersection geometries located upon applying MECX optimization algorithms with these two electronic structure methods. To locate the MECXs (or MECPs) with (LR-TD)DFT/TDA or MP2/ADC(2), we used a combination of different geometry optimization algorithms to ensure that the lowest possible electronic energy was found for these critical points. For (LR-TD)DFT/TDA, the gradient-projection method presented in the work of Bearpark *et al.*,¹³⁹ the Lagrange–Newton method of Manaa and Yarkony,¹⁴¹ the penalty-function of Ciminelli *et al.*,¹⁴² and the CIOpt method of Levine *et al.*²² were used; CIOpt was used for MP2/ADC(2) with subsequent refinement of the MECX (or MECP) geometries carried out within their respective branching spaces. The details of these procedures can be found in the supplementary material.

It is important to stress here that in each case, the same electronic structure method was used to calculate the electronic energies and to optimize the three critical geometries.

b. Pyrazine. The same procedure was used to optimize the critical geometries in pyrazine. Only the S_0 minimum and S_2/S_1 MECX geometries were considered using the three electronic structure methods. Equally, we do not present LIIC plots for pyrazine.

3. Plotting the CX branching space

The branching space vectors, $\mathbf{g}_{ij}(\mathbf{R})$ and $\mathbf{h}_{ij}(\mathbf{R})$, were first computed using XMS-CASPT2 at the optimized XMS-CASPT2 S_j/S_i MECX geometry. The branching space vectors were then orthogonalized by the Yarkony procedure^{20,143} and appropriately normalized, before being used to generate a 2D grid of 29×29 geometries along the branching plane, centered on the optimized XMS-CASPT2 S_j/S_i MECX geometry. To facilitate this, nuclear distortions along the orthonormalized $\tilde{\mathbf{x}}_{ij}(\mathbf{R})$ and $\tilde{\mathbf{y}}_{ij}(\mathbf{R})$ vector directions (see the supplementary material for branching space vector definitions) were multiplied by an appropriate scale factor and added in 14 increments in the positive and negative directions, respectively, spanning ± 0.001 Å in both branching space vector directions, as was done similarly in Ref. 144. At each grid-point geometry, a single-point XMS-CASPT2 energy calculation was performed, giving the S_i and S_j PESs in the region surrounding the optimized XMS-CASPT2 S_j/S_i MECX geometry. Electronic energies are given relative to the S_i energy at the MECX geometry, which is located at the grid origin.

The same procedure was repeated to obtain the corresponding S_j/S_i MECX (or MECP) branching spaces of (LR-TD)DFT/TDA/PBE0 and MP2/ADC(2), respectively. For direct comparison of the branching space plots in Figs. 2–5 (and Figs. S3, S5, S6, and S8 in the supplementary material) obtained by the different electronic structure methods, we followed the approach taken in Ref. 25: The orthonormalized branching space vectors were rotated

within their respective branching planes to ensure maximal overlap with the reference orthonormalized vectors of XMS-CASPT2. These new rotated (orthonormalized) branching space vectors are denoted $\tilde{x}'_{ij}(\mathbf{R})$ and $\tilde{y}'_{ij}(\mathbf{R})$. Details of this rotation procedure and the process used to orthonormalize the raw branching space vectors are provided in the supplementary material.

We stress again that in each case, the same electronic structure method was used to compute the electronic energies and branching space vectors and to optimize the MECX (or MECP) geometries, except for MP2/ADC(2), where the $\mathbf{h}_{ij}(\mathbf{R})$ vector from XMS-CASPT2 was used instead. Therefore, the branching spaces constructed are fully consistent within each electronic structure method, except for the derivative couplings in ADC(2).

4. CX branching space topography parameters

To provide a numerical comparison of the topography of the MECXs obtained by different electronic structure methods in this work, we calculated the CX topography parameters, \mathcal{P} and \mathcal{B} , as defined in Eqs. (57) and (58) of Ref. 145, respectively. For reference, the MECXs are characterized¹⁵ as peaked ($\mathcal{P} < 1$) or sloped ($\mathcal{P} > 1$), and bifurcating ($\mathcal{B} < 1$) or single-path ($\mathcal{B} > 1$)—see the supplementary material for the \mathcal{P} and \mathcal{B} values and MECX characterizations (Table S1) and additional details on the determination of these parameters.

III. RESULTS AND DISCUSSION

A. Protonated formaldimine

The photophysics of protonated formaldimine, CH_2NH_2^+ , has been extensively studied (e.g., Refs. 146–150) due to the molecule

acting as the simplest model system for the chromophore in rhodopsin, the protonated Schiff base of retinal. Within the FC region, protonated formaldimine possesses an optically dark S_1 state and a bright S_2 state of predominantly $\sigma\pi^*$ and $\pi\pi^*$ electronic character, respectively.^{74,118} (We note that the $\sigma\pi^*$ transition is also characterized in the literature as $\pi'\pi^*$, with π' being orthogonal to the π^* orbital.) Given the much higher oscillator strength exhibited by S_2 , photoexcitation occurs predominantly to S_2 , with relaxation to the S_0 ground state involving passage through two subsequent MECXs. The first (S_2/S_1) has been shown to exhibit a peaked topography, while the second (S_1/S_0) has been shown to be sloped.¹¹⁸ Hence, protonated formaldimine constitutes a perfect model system [i.e., possessing MECXs (i) between different types of electronic states and (ii) exhibiting different topographies] to assess the quality of the branching space provided by (LR-TD)DFT/TDA/PBE0 and MP2/ADC(2).

1. Linear interpolation in internal coordinates

In the following, we compare the photochemical pathway of protonated formaldimine by calculating the three lowest electronic state energies along an LIIC pathway connecting the FC, S_2/S_1 MECX, and S_1/S_0 MECX critical geometries obtained with XMS-CASPT2, MP2/ADC(2), and (LR-TD)DFT/TDA/PBE0 (see molecular representation in Fig. 1).

According to XMS-CASPT2 [Fig. 1(a)], following photoexcitation to S_2 , protonated formaldimine decays to S_1 via a strongly peaked S_2/S_1 MECX, which is encountered by a stretch of the C–N bond while retaining the planarity of the molecule exhibited at the FC geometry (S_0 min, 1.281 Å; S_2/S_1 MECX, 1.420 Å).

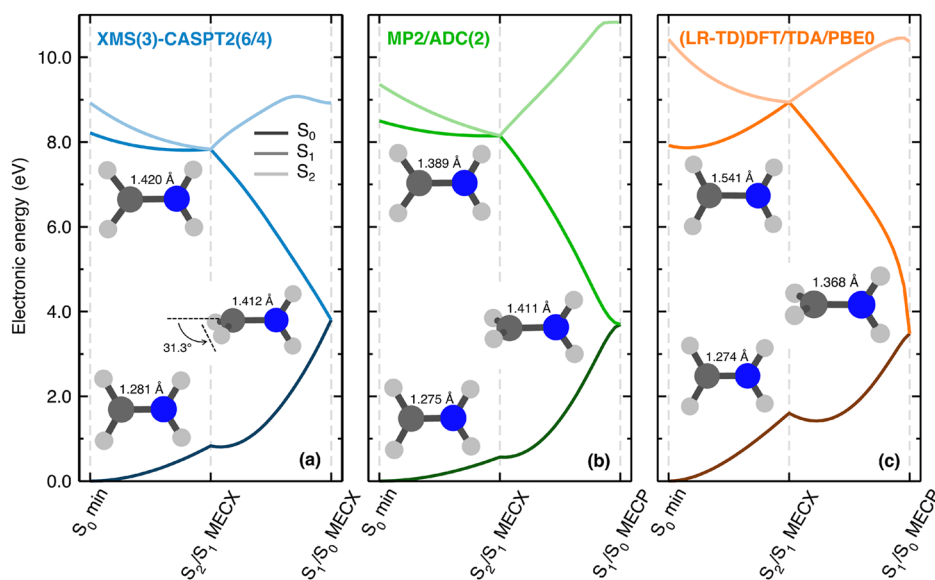


FIG. 1. LIIC pathways connecting the S_0 minimum, S_2/S_1 MECX, and S_1/S_0 MECX (or MECP) in protonated formaldimine. Comparison of the S_0 (dark color), S_1 (mid-color), and S_2 (light color) electronic energies obtained with (a) XMS(3)-CASPT2(6/4)/cc-pVTZ (blue), (b) MP2/ADC(2)/cc-pVTZ (green), and (c) (LR-TD)DFT/TDA/PBE0/cc-pVDZ (orange). In each panel, the critical geometries were optimized at the same level of theory used to compute the electronic energies. The insets show the molecular structures of the three critical points [S_0 min, bottom left; S_2/S_1 MECX, top left; S_1/S_0 MECX (or MECP), middle right] along with the calculated C–N bond lengths [and the CH_2 pyramidalization angle for the XMS(3)-CASPT2(6/4) S_1/S_0 MECX geometry].

Such a peaked topography is assumed to provide highly efficient nonadiabatic population transfer from S_2 to S_1 .¹¹⁸ Subsequent relaxation to the ground electronic state occurs through a weakly sloped S_1/S_0 MECX, which for XMS-CASPT2 is reached via a 90° twist about the C–N bond and an additional 31.3° pyramidalization of the CH_2 moiety. Less efficient S_1 -to- S_0 decay is expected for the predicted sloped topography of the S_1/S_0 MECX.¹¹⁸ Previous investigations with MRCISD have reported purely twisted S_1/S_0 MECX geometries with no CH_2 pyramidalization,^{22,151} whereas others employing MS-CASPT2 have instead predicted the C–N torsion accompanied by pyramidalization of the NH_2 group.²² The differences in S_1/S_0 MECX geometry obtained by different multireference methods have been ascribed to an apparent flatness of the intersection seam with respect to pyramidalization (at either end of the C–N bond).²²

We now compare the XMS-CASPT2 LIIC pathway to those obtained with (LR-TD)DFT/TDA/PBE0 [Fig. 1(c)] and MP2/ADC(2) [Fig. 1(b)]. Considering the overall electronic energy profiles of the different methods along the LIIC, an obvious observation is the striking agreement between MP2/ADC(2) and XMS-CASPT2; the only notable difference is the behavior of S_2 in the segment connecting the two MECXs (explained by the involvement of other electronic states not included in XMS-CASPT2). On the other hand, LR-TDDFT/TDA/PBE0 predicts an $S_2 - S_1$ energy difference at the S_0 minimum over twice that given by either ADC(2) or XMS-CASPT2. This is in spite of the electronic character of S_1 and S_2 at the respective S_2/S_1 MECX geometries in LR-TDDFT/TDA/PBE0 and ADC(2) being in agreement (see Fig. S2 in the supplementary material). We note here that a detailed discussion of the performance of LR-TDDFT/TDA in describing the character of the electronic states of protonated formalimine goes beyond the scope of this work. The approach to the respective MECX (or MECP) points is also markedly different in (LR-TD)DFT/TDA/PBE0 compared to that in the wavefunction-based methods. Notably, the LR-TDDFT/TDA/PBE0 S_1 state approaches the S_1/S_0 MECP too steeply relative to XMS-CASPT2. This observation further corroborates that the LR-TDDFT/TDA first excited electronic state can vary too rapidly in the vicinity of a CX with the ground state, as previously shown in Ref. 65. Interestingly, neither MP2/ADC(2) nor (LR-TD)DFT/TDA/PBE0 predicts the CH_2 pyramidalization exhibited by XMS-CASPT2 for the S_1/S_0 MECX geometry, despite all three geometries being at approximately the same relative energy. Earlier works using (LR-TD)DFT/TDA/PBE presented similar observations.⁷⁴

2. S_2/S_1 branching space

We now focus our attention on the first intersection seam encountered by protonated formalimine upon photoexcitation to S_2 , by calculating the electronic energies with each electronic structure method within the branching space of their respective S_2/S_1 MECX (Fig. 2). All three electronic structure methods correctly predict a conical ($F - 2$)-dimensional intersection between S_1 and S_2 , where the degeneracy is lifted in both branching space vector directions. We stress again (see Sec. II A) that the success of LR-TDDFT/TDA to accurately describe the topology of the S_2/S_1 MECX is *not necessarily guaranteed*. Our results, however, confirm that linear-response $\mathbf{h}_{12}(\mathbf{R})$ vectors do indeed offer

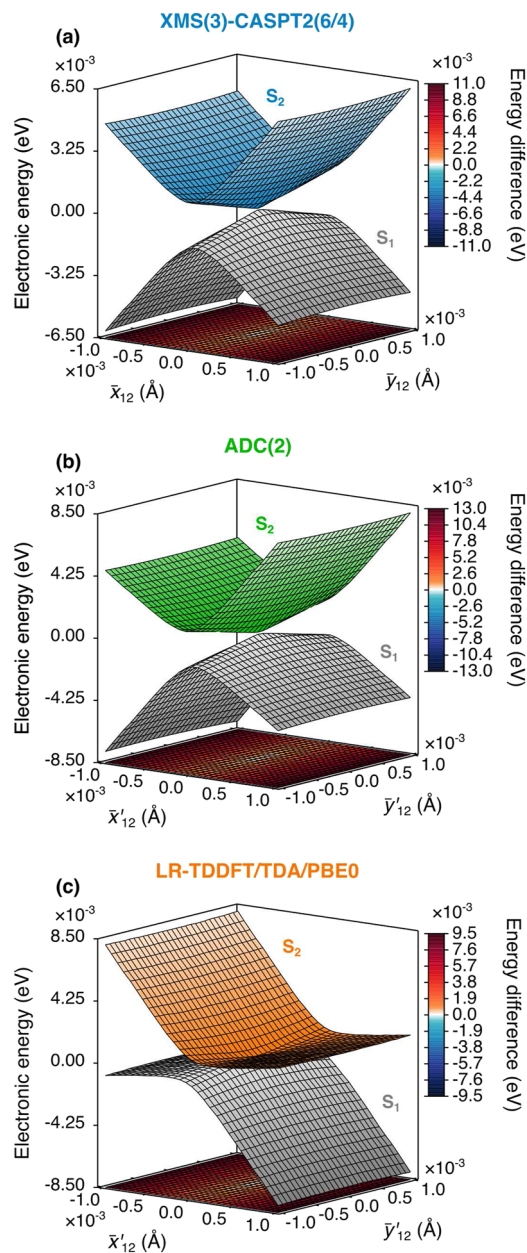


FIG. 2. Branching space of the S_2/S_1 MECX in protonated formalimine. Comparison of the S_1 and S_2 PESs obtained with (a) XMS(3)-CASPT2(6/4)/cc-pVTZ (blue/gray), (b) ADC(2)/cc-pVTZ (green/gray), and (c) LR-TDDFT/TDA/PBE0/cc-pVDZ (orange/gray). In each plot, the MECX geometries and branching space vectors were obtained at the same level of theory used to calculate the electronic energies [except for the ADC(2) plot, which used the $\mathbf{h}_{12}(\mathbf{R})$ vector of XMS(3)-CASPT2(6/4)—see Sec. II B 3 for details]. The base in each plot shows a 2D color map of the $S_2 - S_1$ energy difference (see color bar on the right).

an adequate description of the CX branching space in protonated formalimine.

We note that the S_1 and S_2 PESs obtained with LR-TDDFT/TDA/PBE0 are in relatively poor agreement with those of

the XMS-CASPT2 reference [compare Figs. 2(a) and 2(c)]. Using the CX branching space topography parameters defined in Ref. 145 (see Sec. II B 4), both methods yield a peaked bifurcating topography, but LR-TDDFT/TDA/PBE0 exhibits larger values of \mathcal{P} and \mathcal{B} (0.59 and 0.86, respectively) than XMS-CASPT2 (0.02 and 0.29). These parameters are summarized in the supplementary material. This disparity between LR-TDDFT/TDA/PBE0 and XMS-CASPT2 links to the LIIC plots in Fig. 1, where the approach of the LR-TDDFT/TDA/PBE0 S_2 and S_1 states (i.e., the $S_2 - S_1$ energy gap and slope of the S_2 and S_1 energies) toward the S_2/S_1 MECX is markedly different in LR-TDDFT/TDA/PBE0 to that in either XMS-CASPT2 or ADC(2). On the other hand, the S_1 and S_2 PESs obtained with ADC(2) are in close agreement with those of XMS-CASPT2; ADC(2) also yields a peaked bifurcating topography for the S_2/S_1 MECX [compare Figs. 2(a) and 2(b)] with similar parameter values of $\mathcal{P} = 0.08$ and $\mathcal{B} = 0.45$. The ability of ADC(2) to adequately describe the branching space of a CX between excited electronic states is reassuring, given its extended use within excited-state molecular dynamics simulations.^{63,152–167} Despite the difference in the abilities of LR-TDDFT/TDA/PBE0 and ADC(2) to closely reproduce the XMS-CASPT2 S_2/S_1 MECX branching space in Fig. 2, the branching space vectors of LR-TDDFT/TDA/PBE0 show a striking resemblance to those of ADC(2) (/XMS-CASPT2)—see Fig. S2 in the supplementary material.

3. S_1/S_0 branching space

Next, we take the opportunity to focus on the performance of the methods in describing the S_1/S_0 MECX branching space of protonated formalimine. XMS-CASPT2 gives a conical ($F - 2$)-dimensional intersection as expected [Fig. 3(a)], with a sloped single-path topography (with parameters, $\mathcal{P} = 1.49$ and $\mathcal{B} = 1.32$) similar to that reported in Ref. 118. As expected from the discussion in Sec. II A, (LR-TD)DFT/TDA/PBE0 and MP2/ADC(2) incorrectly predict a linear ($F - 1$)-dimensional intersection at the S_1/S_0 MECP [Figs. 3(c) and 3(b), respectively], where the degeneracy is only lifted along a single branching space vector direction [i.e., $\tilde{y}'_{01}(\mathbf{R})$]. In both cases, the first response (S_1) state becomes lower in energy than the reference (S_0) state, leading to negative excitation energies along certain regions of the branching plane [see color map in Figs. 3(b) and 3(c)]. This observation corroborates earlier results obtained for (LR-TD)DFT⁶⁵ and MP2/ADC(2).⁸¹ When plotted using the same vertical axis energy range (see Fig. S3 in the supplementary material), it is clear that the (LR-TD)DFT/TDA/PBE0 S_1 PES varies too rapidly in the vicinity of the S_1/S_0 MECP compared to that of both XMS-CASPT2 (where a conical intersection is obtained), and MP2/ADC(2) (where a linear seam of intersection is observed). This difference in behavior between the different electronic structure methods is consistent with the LIIC plots in Fig. 1 close to the S_1/S_0 intersection region. [We note that replacing the (LR-TD)DFT branching space vectors used to generate the (LR-TD)DFT S_1/S_0 MECP (and S_2/S_1 MECX) branching space plots in Figs. 2 and 3 with those of XMS-CASPT2 results in no observable difference to the PESs—except for a trivial reflection in the $\tilde{y}'_{ij}(\mathbf{R})$ vector direction.]

Despite indeed being ($F - 1$)-dimensional near the point where the two electronic states become degenerate, the (LR-TD)DFT/TDA/PBE0 intersection in Fig. 3(c) appears significantly more curved than the strictly linear S_1/S_0 intersection of

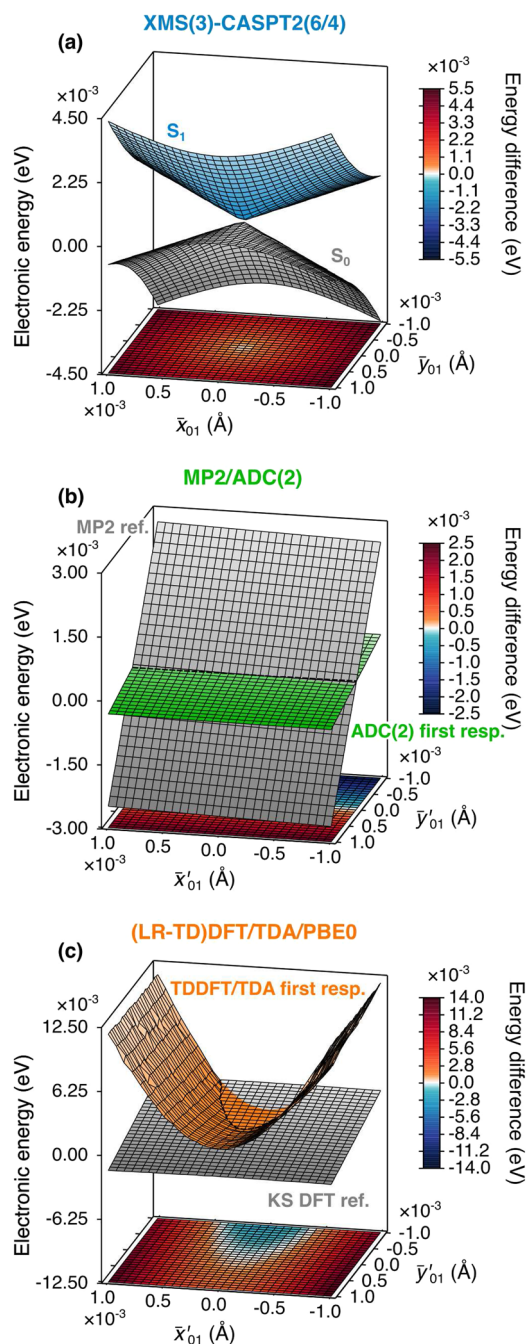


FIG. 3. Branching space of the S_1/S_0 MECX (or MECP) in protonated formalimine. Comparison of the S_0 and S_1 PESs obtained with (a) XMS(3)-CASPT2(6/4)/cc-pVTZ (blue/gray), (b) MP2/ADC(2)/cc-pVTZ (green/gray), and (c) (LR-TD)DFT/TDA/PBE0/cc-pVDZ (orange/gray). In each plot, the MECX (or MECP) geometries and branching space vectors were obtained at the same level of theory used to calculate the electronic energies [except for the MP2/ADC(2) plot, which used the $\mathbf{h}_{01}(\mathbf{R})$ vector of XMS(3)-CASPT2(6/4)—see Sec. II B 3 for details]. The dashed lines in (b) and (c) indicate the seam where $E_0(\mathbf{R}) = E_1(\mathbf{R})$. (We note that the rendering of the colors for the PESs does not reflect precisely this intersection.) The base in each plot shows a 2D color map of the $S_1 - S_0$ energy difference (see color bar on the right).

MP2/ADC(2) in Fig. 3(b). This observation warrants further investigation of the (LR-TD)DFT/TDA/PBE0 intersection at larger distances along the $\tilde{y}'_{01}(\mathbf{R})$ vector direction. Plotting the (LR-TD)DFT/TDA/PBE0 S_0 and S_1 PESs along an extended branching plane [$\pm 0.003 \times \tilde{x}'_{01}(\mathbf{R})$ and $\pm 0.03 \times \tilde{y}'_{01}(\mathbf{R})$ in Fig. 4(b) compared to the original $\pm 0.001 \times \tilde{x}'_{01}(\mathbf{R})$ and $\pm 0.001 \times \tilde{y}'_{01}(\mathbf{R})$ in Fig. 3—see supplementary material for branching space vector definitions] reveals that the curved intersection seam in Fig. 3(c) is in fact just one part of a larger intersection ring—something that shows a striking resemblance to two interpenetrating cones. On the other hand, the strictly linear intersection seam in MP2/ADC(2) observed along the standard branching plane [Fig. 3(b)] remains even along this extended branching plane [Fig. 4(a)]. Overall, our results connect the different pictures proposed earlier for the description of S_1/S_0 MECPs within (LR-TD)DFT/TDA: performing an S_1/S_0 MECP optimization with (LR-TD)DFT/TDA will in fact locate a geometry on the intersection ring and the MECP will look different depending on the extent of the branching space explored to unravel the shape of the S_0 and S_1 PESs around this location—either a (near-to-linear) seam of intersection for minute variations along $\tilde{x}'_{01}(\mathbf{R})$ and $\tilde{y}'_{01}(\mathbf{R})$ [like in Fig. 3(c) and as first reported in the work of Levine *et al.*⁶⁵] or an *intersection ring* (reminiscent of two interpenetrating cones) when a more extended scan along $\tilde{x}'_{01}(\mathbf{R})$ and $\tilde{y}'_{01}(\mathbf{R})$ is performed [like in Fig. 4(b) and as alluded to in the work of Tapavicza *et al.*⁶⁶]. We note that it may be possible to miss the negative-energy region of the intersection ring for more extreme scans around the (LR-TD)DFT/TDA S_1/S_0 intersection point (i.e., if one “zooms out” further from the crossing point), giving a false impression that (LR-TD)DFT/TDA can describe the intersection point adequately.

We conclude this section by noting that we also calculated the HF/CIS S_1/S_0 MECP branching space for both the standard and extended grid of geometries around the intersection point—see Figs. S5 and S6 in the supplementary material. As expected (Sec. II A) HF/CIS predicts a strictly linear ($F - 1$)-dimensional intersection along the standard branching plane that likewise remains along the extended branching plane, which is analogous to the behavior of MP2/ADC(2), but in contrast to that of (LR-TD)DFT/TDA/PBE0. We have confirmed that our (LR-TD)DFT/TDA findings are unaffected by improving the numerical accuracy of our calculations [i.e., increased grid size—see also the supplementary material for details regarding SCF convergence]. These observations solidify our conclusions that the description of CXs involving the ground state by (LR-TD)DFT/TDA and HF/CIS is not completely analogous.

B. Pyrazine

Next, we consider CXs between excited states for a second exemplar molecule, pyrazine. Like for protonated formalimine, the excited electronic states of pyrazine have been well studied, often considered the definitive case for vibronic coupling in aromatic systems; pyrazine is also a precursor to numerous biologically active molecules.^{119,168–174} Within the FC region, the S_1 state in pyrazine exhibits an $n\pi^*$ character and S_2 is of $\pi\pi^*$ character.¹⁷¹ At the XMS-CASPT2 level, the S_2/S_1 MECX is reached (from the planar S_0 minimum geometry) by simultaneous elongation of the C–N and C–C bonds but with an overall stretching of the ring along the axis bisecting the two nitrogen atoms (see Fig. S7 in the supplementary

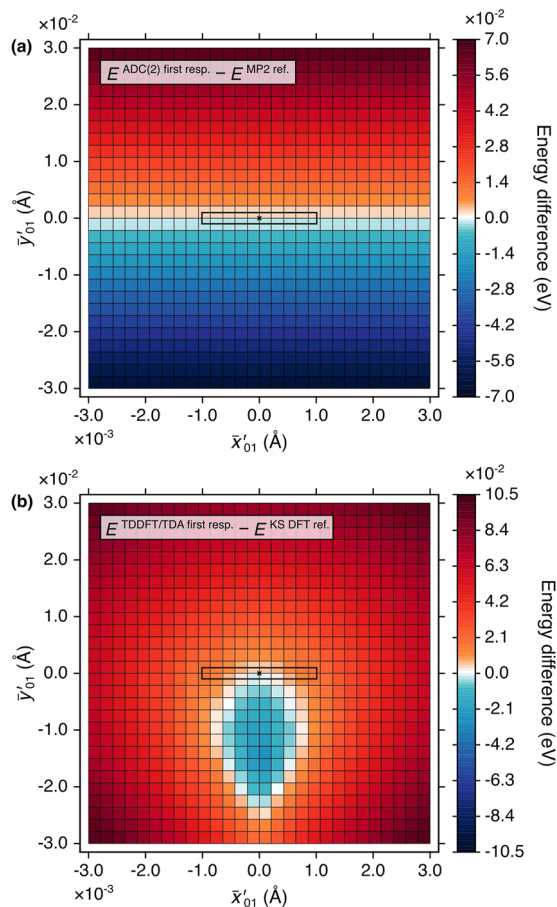


FIG. 4. 2D color map of the electronic energy difference between S_0 (reference state) and S_1 (first response state) obtained with (a) MP2/ADC(2)/cc-pVTZ and (b) (LR-TD)DFT/TDA/PBE0/cc-pVDZ in the vicinity of the S_1/S_0 MECP in protonated formalimine along an extended branching plane [$\pm 0.003 \times \tilde{x}'_{01}(\mathbf{R})$, $\pm 0.03 \times \tilde{y}'_{01}(\mathbf{R})$]. The black box encloses the area spanned by the branching plane used to generate the plots in Fig. 3; the black cross indicates the location of the MECP geometry.

material). LR-TDDFT/TDA/PBE0 and ADC(2) predict S_0 minimum and S_2/S_1 MECX geometries that agree closely with those of XMS-CASPT2. The only difference is the stretching of the S_2/S_1 MECX geometry observed in LR-TDDFT/TDA/PBE0 is slightly more exaggerated than in the wavefunction-based methods, as indicated by the larger (smaller) N–C–C (C–N–C) bond angles. This distortion in the LR-TDDFT/TDA/PBE0 S_2/S_1 MECX geometries is accompanied by it being ~ 1 eV higher in energy than the S_2/S_1 MECX geometry in either XMS-CASPT2 or ADC(2).

1. S_2/S_1 branching space

We focus on the respective branching spaces for the S_2/S_1 MECX (Fig. 5). As for protonated formalimine, all three methods correctly predict a conical ($F - 2$)-dimensional intersection between S_1 and S_2 , where the degeneracy is lifted along both branching space

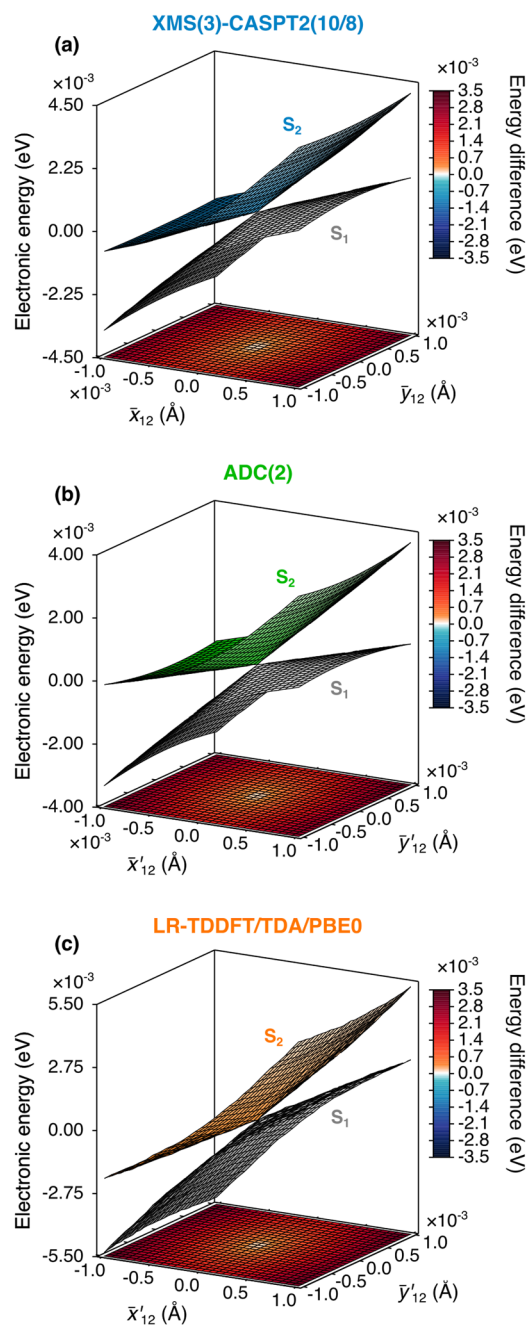


FIG. 5. Branching space of the S_2/S_1 MECX in pyrazine. Comparison of the S_1 and S_2 PESs obtained with (a) XMS(3)-CASPT2(10/8)/cc-pVTZ (blue/gray), (b) ADC(2)/cc-pVTZ (green/gray), and (c) LR-TDDFT/TDA/PBE0/cc-pVDZ (orange/gray). In each plot, the MECX geometries and branching space vectors were obtained at the same level of theory used to calculate the electronic energies [except for the ADC(2) plot, which used the $\mathbf{h}_{12}(\mathbf{R})$ vector of XMS-CASPT2(10/8)—see Sec. II B 3 for details]. The base in each plot shows a 2D color map of the $S_2 - S_1$ energy difference (see color bar on the right).

vector directions. LR-TDDFT/TDA/PBE0 exhibits a sloped single-path MECX, mirroring the topography observed with both XMS-CASPT2 and ADC(2), with \mathcal{P} and \mathcal{B} parameters (7.16 and 2.64, respectively) that are closer to those obtained with XMS-CASPT2 (3.57 and 1.96) than ADC(2) (12.78 and 1.14). Recalculating the S_2/S_1 MECX geometry and its corresponding branching space with a different exchange–correlation functional [i.e., the hybrid long-range corrected (LC)- ω PBE, with range-separated parameter $\omega = 0.4 a_0^{-1}$ —see Fig. S8 in the supplementary material] further generalizes our findings and conclusions that LR-TDDFT/TDA can adequately reproduce the dimensionality of a CX between excited electronic states.

IV. CONCLUSION

This work has shown explicitly that LR-TDDFT/TDA/PBE0 within the AA is able to exhibit the correct topology of a CX between two *excited* electronic states for two exemplar molecules: protonated formalimine and pyrazine. The correct CX topology was unchanged when an alternative exchange–correlation functional was investigated for pyrazine. We further showed that ADC(2) offers an accurate description of both the topology and topography of CXs between excited electronic states and note that this is in contrast to that of (conventional) coupled cluster theory, which can be flawed in this context.^{51,63,175–177} We stress that all CX branching spaces analyzed in this work were constructed within a fully consistent approach where all required electronic quantities were computed at the same level of theory [except for the derivative coupling vectors in ADC(2)].

Re-inspection of the problem faced by AA (LR-TD)DFT/TDA to adequately describe CXs involving the ground electronic states also proved fruitful. Our findings for protonated formalimine show that the two, supposedly different, pictures related to the S_1/S_0 MECP branching space of AA (LR-TD)DFT/TDA/PBE0—a seam of intersection vs two interpenetrating cones—both emanate from the intersection ring, which can be reconciled by analyzing the behavior of the PESs, either in the immediate vicinity of the S_1/S_0 MECP or at further distances from the MECP geometry. The intersection ring from AA (LR-TD)DFT/TDA/PBE0 is in stark contrast to the linear intersection observed from MP2/ADC(2) (and, as expected, HF/CIS). Further work is arguably still needed to pinpoint precisely how nonadiabatic dynamics simulations is influenced by the intersection ring and whether the difference in behavior of AA (LR-TD)DFT/TDA/PBE0 to that of HF/CIS gives any grounds for optimism when applying AA (LR-TD)DFT/TDA in this context. Again, extending the use of previously proposed expressions for the (exact) frequency-dependent exchange–correlation kernel^{78,97,98,178–184} to the problem of CXs involving the ground electronic state still remains as pertinent as ever. Nonetheless, for the case of CXs between excited electronic states, greater confidence (at least for electronic states dominated by single excitations) should be felt when applying AA LR-TDDFT/TDA to chemically (and biologically) relevant systems, whose size still prohibits the use of multiconfigurational methods.

SUPPLEMENTARY MATERIAL

The supplementary material contains additional details on the electronic structure methods, the determination of critical points and LIICs pathways, and the plotting of the CX branching spaces. Additional figures are provided on the active space orbitals, the electronic-state characters at the S_2/S_1 MECX of protonated formalimine, alternative plots of the MECXs branching spaces for protonated formalimine (in particular the S_1/S_0 MECX branching space at the HF/CIS level of theory), and the MECX branching space of pyrazine with a different exchange–correlation functional. A zip file is provided with all the MECX/MECP geometries and branching space vectors presented in this work.

ACKNOWLEDGMENTS

The authors thank Professor Neepa T. Maitra, Professor E. K. U. Gross, and Professor Todd J. Martínez for stimulating discussions. This project has received funding from the European Research Council (ERC) under the European Union's Horizon 2020 research and innovation programme (Grant Agreement No. 803718, project SINDAM) and the EPSRC Grant No. EP/V026690/1. J.T.T. acknowledges the EPSRC for an EPSRC Doctoral Studentship (Grant No. EP/T518001/1). This work made use of the facilities of the Hamilton HPC Service of Durham University.

AUTHOR DECLARATIONS

Conflict of Interest

The authors have no conflicts to disclose.

Author Contributions

Jack T. Taylor: Formal analysis (lead); Investigation (lead); Methodology (equal); Validation (lead); Visualization (lead); Writing – original draft (lead); Writing – review & editing (equal). **David J. Tozer:** Funding acquisition (equal); Methodology (equal); Supervision (equal); Writing – review & editing (equal). **Basile F. E. Curchod:** Conceptualization (lead); Funding acquisition (equal); Methodology (equal); Supervision (equal); Writing – review & editing (equal).

DATA AVAILABILITY

The data that support the findings of this study are available within the article and its supplementary material.

REFERENCES

- M. Born and K. Huang, *Dynamical Theory of Crystal Lattices*, Oxford Classic Texts in the Physical Sciences (Clarendon Press; Oxford University Press, Oxford; New York, 1988).
- J. V. Neumann and E. Wigner, *World Scientific Series in 20th Century Chemistry* (World Scientific, 2000), Vol. 8, pp. 25–31.
- E. Teller, *J. Phys. Chem.* **41**, 109 (1937).
- G. Herzberg and H. C. Longuet-Higgins, *Discuss. Faraday Soc.* **35**, 77 (1963).
- W. T. A. M. Van der Lugt and L. J. Oosterhoff, *J. Am. Chem. Soc.* **91**, 6042 (1969).

- J. Michl, *Fortschritte der Chemischen Forschung: Photochemistry, Topics in Current Chemistry* (Springer, Berlin, Heidelberg, 1974), pp. 1–59.
- D. G. Truhlar and C. A. Mead, *Phys. Rev. A* **68**, 032501 (2003).
- B. G. Levine and T. J. Martínez, *Annu. Rev. Phys. Chem.* **58**, 613 (2007).
- D. R. Yarkony, *Chem. Rev.* **112**, 481 (2012).
- S. Matsika and P. Krause, *Annu. Rev. Phys. Chem.* **62**, 621 (2011).
- Y. Boeije and M. Olivucci, *Chem. Soc. Rev.* **52**, 2643 (2023).
- M. Riad Manaa and D. R. Yarkony, *J. Chem. Phys.* **93**, 4473 (1990).
- F. Bernardi, S. De, M. Olivucci, and M. A. Robb, *J. Am. Chem. Soc.* **112**, 1737 (1990).
- S. S. Xantheas, G. J. Atchity, S. T. Elbert, and K. Ruedenberg, *J. Chem. Phys.* **94**, 8054 (1991).
- G. J. Atchity, S. S. Xantheas, and K. Ruedenberg, *J. Chem. Phys.* **95**, 1862 (1991).
- D. Polli, P. Altoè, O. Weingart, K. M. Spillane, C. Manzoni, D. Brida, G. Tomasello, G. Orlandi, P. Kukura, R. A. Mathies, M. Garavelli, and G. Cerullo, *Nature* **467**, 440 (2010).
- T. J. Martínez, *Nature* **467**, 412 (2010).
- L. M. Frutos, T. Andruniów, F. Santoro, N. Ferré, and M. Olivucci, *Proc. Natl. Acad. Sci. U. S. A.* **104**, 7764 (2007).
- In other words, if either a diabatic electronic basis or the exact-factorization representation of the molecular wavefunction were used instead, CXs would not be observed.
- D. R. Yarkony, *J. Phys. Chem. A* **105**, 6277 (2001).
- D. R. Yarkony, *Rev. Mod. Phys.* **68**, 985 (1996).
- B. G. Levine, J. D. Coe, and T. J. Martínez, *J. Phys. Chem. B* **112**, 405 (2008).
- S. Gozem, F. Melaccio, A. Valentini, M. Filatov, M. Huix-Rotllant, N. Ferré, L. M. Frutos, C. Angeli, A. I. Krylov, A. A. Granovsky, R. Lindh, and M. Olivucci, *J. Chem. Theory Comput.* **10**, 3074 (2014).
- S. Matsika, *Chem. Rev.* **121**, 9407 (2021).
- F. Liu, M. Filatov, and T. J. Martínez, *J. Chem. Phys.* **154**, 104108 (2021).
- A. A. Granovsky, *J. Chem. Phys.* **134**, 214113 (2011).
- S. Gozem, M. Huntress, I. Schapiro, R. Lindh, A. A. Granovsky, C. Angeli, and M. Olivucci, *J. Chem. Theory Comput.* **8**, 4069 (2012).
- S. Sen and I. Schapiro, *Mol. Phys.* **116**, 2571 (2018).
- J. W. Park, *J. Chem. Theory Comput.* **16**, 326 (2020).
- S. Battaglia and R. Lindh, *J. Chem. Phys.* **154**, 034102 (2021).
- Y. Nishimoto, S. Battaglia, and R. Lindh, *J. Chem. Theory Comput.* **18**, 4269 (2022).
- B. O. Roos, P. R. Taylor, and P. E. Sigbahn, *Chem. Phys.* **48**, 157 (1980).
- J. W. Park and T. Shiozaki, *J. Chem. Theory Comput.* **13**, 3676 (2017).
- I. Polyak, L. Hutton, R. Crespo-Otero, M. Barbatti, and P. J. Knowles, *J. Chem. Theory Comput.* **15**, 3929 (2019).
- M. Heindl and L. González, *Comput. Theor. Chem.* **1155**, 38 (2019).
- J. W. Park, *J. Chem. Theory Comput.* **15**, 3960 (2019).
- M. Winslow, W. B. Cross, and D. Robinson, *J. Chem. Theory Comput.* **16**, 3253 (2020).
- P. Chakraborty, Y. Liu, T. Weinacht, and S. Matsika, *Faraday Discuss.* **228**, 266 (2021).
- L. Zhang, Y. Shu, S. Bhaumik, X. Chen, S. Sun, Y. Huang, and D. G. Truhlar, *J. Chem. Theory Comput.* **18**, 7073 (2022).
- K. Andersson, P. Å. Malmqvist, B. O. Roos, A. J. Sadlej, and K. Wolinski, *J. Phys. Chem.* **94**, 5483 (1990).
- K. Andersson, P. Å. Malmqvist, and B. O. Roos, *J. Chem. Phys.* **96**, 1218 (1992).
- J. Finley, P. Å. Malmqvist, B. O. Roos, and L. Serrano-Andrés, *Chem. Phys. Lett.* **288**, 299 (1998).
- T. Shiozaki, W. Györffy, P. Celani, and H.-J. Werner, *J. Chem. Phys.* **135**, 081106 (2011).
- E. Runge and E. K. U. Gross, *Phys. Rev. Lett.* **52**, 997 (1984).
- M. E. Casida, *Recent Advances in Computational Chemistry* (World Scientific, 1995), Vol. 1, pp. 155–192.
- M. Petersilka, U. J. Gossmann, and E. K. U. Gross, *Phys. Rev. Lett.* **76**, 1212 (1996).
- C. A. Ullrich, *Time-Dependent Density-Functional Theory: Concepts and Applications* (Oxford University Press, 2011).

- ⁴⁸J. Schirmer, *Phys. Rev. A* **26**, 2395 (1982).
- ⁴⁹A. B. Trofimov and J. Schirmer, *J. Phys. B: At., Mol. Opt. Phys.* **28**, 2299 (1995).
- ⁵⁰A. Dreuw and M. Wormit, *Wiley Interdiscip. Rev.: Comput. Mol. Sci.* **5**, 82 (2015).
- ⁵¹C. Hättig, *Structure Optimizations for Excited States with Correlated Second-Order Methods: CC2 and ADC(2)*, Advances in Quantum Chemistry Vol. 50 (Elsevier, 2005), pp. 37–60.
- ⁵²J. F. Stanton and R. J. Bartlett, *J. Chem. Phys.* **98**, 7029 (1993).
- ⁵³D. C. Comeau and R. J. Bartlett, *Chem. Phys. Lett.* **207**, 414 (1993).
- ⁵⁴O. Christiansen, H. Koch, and P. Jørgensen, *Chem. Phys. Lett.* **243**, 409 (1995).
- ⁵⁵A. I. Krylov, *Chem. Phys. Lett.* **338**, 375 (2001).
- ⁵⁶A. I. Krylov, *Acc. Chem. Res.* **39**, 83 (2006).
- ⁵⁷A. I. Krylov, *Annu. Rev. Phys. Chem.* **59**, 433 (2008).
- ⁵⁸K. Sneskov and O. Christiansen, *Wiley Interdiscip. Rev.: Comput. Mol. Sci.* **2**, 566 (2012).
- ⁵⁹S. Hirata and M. Head-Gordon, *Chem. Phys. Lett.* **302**, 375 (1999).
- ⁶⁰E. Tapavicza, I. Tavernelli, and U. Rothlisberger, *Phys. Rev. Lett.* **98**, 023001 (2007).
- ⁶¹U. Werner, R. Mitrić, T. Suzuki, and V. Bonačić-Koutecký, *Chem. Phys.* **349**, 319 (2008).
- ⁶²B. F. E. Curchod, U. Rothlisberger, and I. Tavernelli, *ChemPhysChem* **14**, 1314 (2013).
- ⁶³F. Plasser, R. Crespo-Otero, M. Pederzoli, J. Pittner, H. Lischka, and M. Barbatti, *J. Chem. Theory Comput.* **10**, 1395 (2014).
- ⁶⁴R. Crespo-Otero and M. Barbatti, *Chem. Rev.* **118**, 7026 (2018).
- ⁶⁵B. G. Levine, C. Ko, J. Quenneville, and T. J. Martínez, *Mol. Phys.* **104**, 1039 (2006).
- ⁶⁶E. Tapavicza, I. Tavernelli, U. Rothlisberger, C. Filippi, and M. E. Casida, *J. Chem. Phys.* **129**, 124108 (2008).
- ⁶⁷M. Huix-Rotllant, M. Filatov, S. Gozem, I. Schapiro, M. Olivucci, and N. Ferré, *J. Chem. Theory Comput.* **9**, 3917 (2013).
- ⁶⁸M. Huix-Rotllant, A. Nikiforov, W. Thiel, and M. Filatov, *Top. Curr. Chem.* **368**, 445 (2015).
- ⁶⁹M. Barbatti and R. Crespo-Otero, *Top. Curr. Chem.* **368**, 415 (2015).
- ⁷⁰M. E. Casida, B. Natarajan, and T. Deutsch, in *Fundamentals of Time-Dependent Density Functional Theory*, edited by M. A. Marques, N. T. Maitra, F. M. Nogueira, E. Gross, and A. Rubio (Springer, Berlin, Heidelberg, 2012), Vol. 837, pp. 279–299.
- ⁷¹S. Fantacci, A. Migani, and M. Olivucci, *J. Phys. Chem. A* **108**, 1208 (2004).
- ⁷²A. Szabo and N. S. Ostlund, *Modern Quantum Chemistry: Introduction to Advanced Electronic Structure Theory*, 1st ed. (Dover Publications, Mineola, NY, 1996).
- ⁷³X. Zhang and J. M. Herbert, *J. Chem. Phys.* **155**, 124111 (2021).
- ⁷⁴I. Tavernelli, E. Tapavicza, and U. Rothlisberger, *J. Mol. Struct.: THEOCHEM* **914**, 22 (2009).
- ⁷⁵A. J. Cohen, D. J. Tozer, and N. C. Handy, *J. Chem. Phys.* **126**, 214104 (2007).
- ⁷⁶J. A. Pople, P. M. W. Gill, and N. C. Handy, *Int. J. Quantum Chem.* **56**, 303 (1995).
- ⁷⁷Y. Yang, L. Shen, D. Zhang, and W. Yang, *J. Phys. Chem. Lett.* **7**, 2407 (2016).
- ⁷⁸M. E. Casida and M. Huix-Rotllant, *Top. Curr. Chem.* **368**, 1 (2015).
- ⁷⁹B. Kaduk and T. Van Voorhis, *J. Chem. Phys.* **133**, 061102 (2010).
- ⁸⁰J. M. Herbert and A. Mandal, *Time-Dependent Density Functional Theory: Nonadiabatic Molecular Dynamics* (Jenny Stanford Publishing, 2022).
- ⁸¹D. Tuna, D. Lefrançois, Ł. Wolański, S. Gozem, I. Schapiro, T. Andruniów, A. Dreuw, and M. Olivucci, *J. Chem. Theory Comput.* **11**, 5758 (2015).
- ⁸²H.-H. Teh and J. E. Subotnik, *J. Phys. Chem. Lett.* **10**, 3426 (2019).
- ⁸³V. Athavale, H.-H. Teh, and J. E. Subotnik, *J. Chem. Phys.* **155**, 154105 (2021).
- ⁸⁴S. L. Li, A. V. Marenich, X. Xu, and D. G. Truhlar, *J. Phys. Chem. Lett.* **5**, 322 (2014).
- ⁸⁵Y. Shu, K. A. Parker, and D. G. Truhlar, *J. Phys. Chem. Lett.* **8**, 2107 (2017).
- ⁸⁶Y. Shu, K. A. Parker, and D. G. Truhlar, *J. Phys. Chem. A* **121**, 9728 (2017).
- ⁸⁷J. M. Herbert, X. Zhang, A. F. Morrison, and J. Liu, *Acc. Chem. Res.* **49**, 931 (2016).
- ⁸⁸J. M. Herbert, *Theoretical and Computational Photochemistry* (Elsevier, 2023), pp. 69–118.
- ⁸⁹Y. A. Bernard, Y. Shao, and A. I. Krylov, *J. Chem. Phys.* **136**, 204103 (2012).
- ⁹⁰Y. Shao, M. Head-Gordon, and A. I. Krylov, *J. Chem. Phys.* **118**, 4807 (2003).
- ⁹¹H. van Aggelen, Y. Yang, and W. Yang, *Phys. Rev. A* **88**, 030501 (2013).
- ⁹²Y. Yang, H. van Aggelen, and W. Yang, *J. Chem. Phys.* **139**, 224105 (2013).
- ⁹³Y. Yang, D. Peng, J. Lu, and W. Yang, *J. Chem. Phys.* **141**, 124104 (2014).
- ⁹⁴C. Bannwarth, J. K. Yu, E. G. Hohenstein, and T. J. Martínez, *J. Chem. Phys.* **153**, 024110 (2020).
- ⁹⁵J. K. Yu, C. Bannwarth, E. G. Hohenstein, and T. J. Martínez, *J. Chem. Theory Comput.* **16**, 5499 (2020).
- ⁹⁶We note, this is in contrast to the situation in CIS, where the equations are always linear and only ever approximate (i.e., the exact case would be full CI). Even within the AA, where now the LR-TDDFT equations are indeed linear, the response matrix elements in AA LR-TDDFT/(TDA) differ from that in CIS, where the former depends on the response of the multiplicative exchange–correlation potential, whereas the latter depends on the response of the non-multiplicative HF exchange potential.
- ⁹⁷J. Authier and P.-F. Loos, *J. Chem. Phys.* **153**, 184105 (2020).
- ⁹⁸P. Romaniello, D. Sangalli, J. A. Berger, F. Sottile, L. G. Molinari, L. Reining, and G. Onida, *J. Chem. Phys.* **130**, 044108 (2009).
- ⁹⁹N. T. Maitra, *J. Chem. Phys.* **122**, 234104 (2005).
- ¹⁰⁰N. T. Maitra and D. G. Tempel, *J. Chem. Phys.* **125**, 184111 (2006).
- ¹⁰¹It should be noted that Levine *et al.* did provide a very brief discussion about the description of CXs between excited states with AA LR-TDDFT for molecules, such as malonaldehyde and benzene, within their seminal work (Ref. 65). However, no explicit branching space plots were presented.
- ¹⁰²V. Chernyak and S. Mukamel, *J. Chem. Phys.* **112**, 3572 (2000).
- ¹⁰³M. Baer, *Phys. Rep.* **358**, 75 (2002).
- ¹⁰⁴R. Send and F. Furche, *J. Chem. Phys.* **132**, 044107 (2010).
- ¹⁰⁵C. Hu, H. Hirai, and O. Sugino, *J. Chem. Phys.* **127**, 064103 (2007).
- ¹⁰⁶I. Tavernelli, E. Tapavicza, and U. Rothlisberger, *J. Chem. Phys.* **130**, 124107 (2009).
- ¹⁰⁷I. Tavernelli, B. F. E. Curchod, and U. Rothlisberger, *J. Chem. Phys.* **131**, 196101 (2009).
- ¹⁰⁸I. Tavernelli, B. F. E. Curchod, A. Laktionov, and U. Rothlisberger, *J. Chem. Phys.* **133**, 194104 (2010).
- ¹⁰⁹Z. Li and W. Li, *J. Chem. Phys.* **141**, 014110 (2014).
- ¹¹⁰Z. Li, B. Suo, and W. Liu, *J. Chem. Phys.* **141**, 244105 (2014).
- ¹¹¹Z. Wang, C. Wu, and W. Liu, *Acc. Chem. Res.* **54**, 3288 (2021).
- ¹¹²S. M. Parker, S. Roy, and F. Furche, *Phys. Chem. Chem. Phys.* **21**, 18999 (2019).
- ¹¹³Q. Ou, E. C. Alguire, and J. E. Subotnik, *J. Phys. Chem. B* **119**, 7150 (2015).
- ¹¹⁴B. Vlaisavljevich and T. Shiozaki, *J. Chem. Theory Comput.* **12**, 3781 (2016).
- ¹¹⁵J. W. Park and T. Shiozaki, *J. Chem. Theory Comput.* **13**, 2561 (2017).
- ¹¹⁶T. Shiozaki, *Wiley Interdiscip. Rev.: Comput. Mol. Sci.* **8**, e1331 (2018).
- ¹¹⁷R. Lindh and I. F. Galván, in *Quantum Chemistry and Dynamics of Excited States*, 1st ed., edited by L. González and R. Lindh (Wiley, 2020), pp. 299–353.
- ¹¹⁸M. Barbatti, A. J. A. Aquino, and H. Lischka, *Mol. Phys.* **104**, 1053 (2006).
- ¹¹⁹T. Shiozaki, C. Woywod, and H.-J. Werner, *Phys. Chem. Chem. Phys.* **15**, 262 (2013).
- ¹²⁰P. Hohenberg and W. Kohn, *Phys. Rev.* **136**, B864 (1964).
- ¹²¹W. Kohn and L. J. Sham, *Phys. Rev.* **140**, A1133 (1965).
- ¹²²R. G. Parr and Y. Weitao, *Density-Functional Theory of Atoms and Molecules* (Oxford University Press, 1989).
- ¹²³C. M. Isborn, N. Luehr, I. S. Ufimtsev, and T. J. Martínez, *J. Chem. Theory Comput.* **7**, 1814 (2011).
- ¹²⁴I. S. Ufimtsev and T. J. Martínez, *J. Chem. Theory Comput.* **4**, 222 (2008).
- ¹²⁵I. S. Ufimtsev and T. J. Martínez, *J. Chem. Theory Comput.* **5**, 2619 (2009).
- ¹²⁶I. S. Ufimtsev and T. J. Martínez, *J. Chem. Theory Comput.* **5**, 3138 (2009).
- ¹²⁷A. V. Titov, I. S. Ufimtsev, N. Luehr, and T. J. Martínez, *J. Chem. Theory Comput.* **9**, 213 (2013).

- ¹²⁸S. Seritan, C. Bannwarth, B. S. Fales, E. G. Hohenstein, S. I. L. Kokkila-Schumacher, N. Luehr, J. W. Snyder, C. Song, A. V. Titov, I. S. Ufimtsev, and T. J. Martínez, *J. Chem. Phys.* **152**, 224110 (2020).
- ¹²⁹S. Seritan, C. Bannwarth, B. S. Fales, E. G. Hohenstein, C. M. Isborn, S. I. L. Kokkila-Schumacher, X. Li, F. Liu, N. Luehr, J. W. Snyder, C. Song, A. V. Titov, I. S. Ufimtsev, L. Wang, and T. J. Martínez, *Wiley Interdiscip. Rev.: Comput. Mol. Sci.* **11**, e1494 (2021).
- ¹³⁰J. P. Perdew, K. Burke, and M. Ernzerhof, *Phys. Rev. Lett.* **77**, 3865 (1996).
- ¹³¹C. Adamo and V. Barone, *J. Chem. Phys.* **110**, 6158 (1999).
- ¹³²M. Ernzerhof and G. E. Scuseria, *J. Chem. Phys.* **110**, 5029 (1999).
- ¹³³C. Møller and M. S. Plesset, *Phys. Rev.* **46**, 618 (1934).
- ¹³⁴C. Hättig, A. Hellweg, and A. Köhn, *Phys. Chem. Chem. Phys.* **8**, 1159 (2006).
- ¹³⁵R. Ahlrichs, M. Bär, M. Häser, H. Horn, and C. Kölmel, *Chem. Phys. Lett.* **162**, 165 (1989).
- ¹³⁶F. Furche, R. Ahlrichs, C. Hättig, W. Klopper, M. Sierka, and F. Weigend, *Wiley Interdiscip. Rev.: Comput. Mol. Sci.* **4**, 91 (2014).
- ¹³⁷F. Weigend, A. Köhn, and C. Hättig, *J. Chem. Phys.* **116**, 3175 (2002).
- ¹³⁸T. H. Dunning, *J. Chem. Phys.* **90**, 1007 (1989).
- ¹³⁹M. J. Bearpark, M. A. Robb, and H. Bernhard Schlegel, *Chem. Phys. Lett.* **223**, 269 (1994).
- ¹⁴⁰H. R. Hudock, B. G. Levine, A. L. Thompson, H. Satzger, D. Townsend, N. Gador, S. Ullrich, A. Stolow, and T. J. Martínez, *J. Phys. Chem. A* **111**, 8500 (2007).
- ¹⁴¹M. R. Manaa and D. R. Yarkony, *J. Chem. Phys.* **99**, 5251 (1993).
- ¹⁴²C. Ciminelli, G. Granucci, and M. Persico, *Chem. - Eur. J.* **10**, 2327 (2004).
- ¹⁴³D. R. Yarkony, *J. Chem. Phys.* **112**, 2111 (2000).
- ¹⁴⁴D. Lefrançois, D. Tuna, T. J. Martínez, and A. Dreuw, *J. Chem. Theory Comput.* **13**, 4436 (2017).
- ¹⁴⁵I. Fdez Galván, M. G. Delcey, T. B. Pedersen, F. Aquilante, and R. Lindh, *J. Chem. Theory Comput.* **12**, 3636 (2016).
- ¹⁴⁶V. Bonačić-Koutecký, K. Schöffel, and J. Michl, *Theor. Chim. Acta* **72**, 459 (1987).
- ¹⁴⁷V. Bonačić-Koutecký, J. Koutecký, and J. Michl, *Angew. Chem., Int. Ed.* **26**, 170 (1987).
- ¹⁴⁸P. Du, S. C. Racine, and E. R. Davidson, *J. Phys. Chem.* **94**, 3944 (1990).
- ¹⁴⁹S. El-Taher, R. H. Hilal, and T. A. Albright, *Int. J. Quantum Chem.* **82**, 242 (2001).
- ¹⁵⁰A. J. A. Aquino, M. Barbatti, and H. Lischka, *ChemPhysChem* **7**, 2089 (2006).
- ¹⁵¹A. Nikiforov, J. A. Gamez, W. Thiel, M. Huix-Rotllant, and M. Filatov, *J. Chem. Phys.* **141**, 124122 (2014).
- ¹⁵²K. Bennett, M. Kowalewski, and S. Mukamel, *J. Chem. Theory Comput.* **12**, 740 (2016).
- ¹⁵³M. A. Kochman and B. Durbeej, *J. Phys. Chem. A* **123**, 6660 (2019).
- ¹⁵⁴M. Sapunar, A. Ponzi, S. Chaiwongwattana, M. Mališ, A. Prlj, P. Decleva, and N. Došlić, *Phys. Chem. Chem. Phys.* **17**, 19012 (2015).
- ¹⁵⁵A. Prlj, B. F. E. Curchod, and C. Corminboeuf, *Phys. Chem. Chem. Phys.* **17**, 14719 (2015).
- ¹⁵⁶M. A. Kochman and B. Durbeej, *J. Phys. Chem. A* **124**, 2193 (2020).
- ¹⁵⁷F. Siddique, M. Barbatti, Z. Cui, H. Lischka, and A. J. A. Aquino, *J. Phys. Chem. A* **124**, 3347 (2020).
- ¹⁵⁸M. Barbatti, *J. Am. Chem. Soc.* **136**, 10246 (2014).
- ¹⁵⁹H. Lischka, M. Barbatti, F. Siddique, A. Das, and A. J. Aquino, *Chem. Phys.* **515**, 472 (2018).
- ¹⁶⁰B. Milovanović, J. Novak, M. Etinski, W. Domcke, and N. Došlić, *Phys. Chem. Chem. Phys.* **23**, 2594 (2021).
- ¹⁶¹A. Prlj, A. Fabrizio, and C. Corminboeuf, *Phys. Chem. Chem. Phys.* **18**, 32668 (2016).
- ¹⁶²J. Novak, A. Prlj, N. Basarić, C. Corminboeuf, and N. Došlić, *Chem. - Eur. J.* **23**, 8244 (2017).
- ¹⁶³M. Dommert and R. Crespo-Otero, *Phys. Chem. Chem. Phys.* **19**, 2409 (2017).
- ¹⁶⁴G. Gate, R. Szabla, M. R. Haggmark, J. Šponer, A. L. Sobolewski, and M. S. De Vries, *Phys. Chem. Chem. Phys.* **21**, 13474 (2019).
- ¹⁶⁵M. A. Kochman, M. Pola, and R. J. D. Miller, *J. Phys. Chem. A* **120**, 6200 (2016).
- ¹⁶⁶L. Hutton and B. F. E. Curchod, *ChemPhotoChem* **6**, e20220015 (2022).
- ¹⁶⁷R. Szabla, R. W. Góra, and J. Šponer, *Phys. Chem. Chem. Phys.* **18**, 20208 (2016).
- ¹⁶⁸C. Woywod, A. Papp, G. J. Halász, and Á. Vibók, *Theor. Chem. Acc.* **125**, 521 (2010).
- ¹⁶⁹G. Stock, C. Woywod, W. Domcke, T. Swinney, and B. S. Hudson, *J. Chem. Phys.* **103**, 6851 (1995).
- ¹⁷⁰M. Sala, S. Guérin, and F. Gatti, *Phys. Chem. Chem. Phys.* **17**, 29518 (2015).
- ¹⁷¹C. Woywod, W. Domcke, A. L. Sobolewski, and H. Werner, *J. Chem. Phys.* **100**, 1400 (1994).
- ¹⁷²M. Kanno, Y. Ito, N. Shimakura, S. Koseki, H. Kono, and Y. Fujimura, *Phys. Chem. Chem. Phys.* **17**, 2012 (2015).
- ¹⁷³A. L. Sobolewski, C. Woywod, and W. Domcke, *J. Chem. Phys.* **98**, 5627 (1993).
- ¹⁷⁴L. Seidner, G. Stock, A. L. Sobolewski, and W. Domcke, *J. Chem. Phys.* **96**, 5298 (1992).
- ¹⁷⁵A. Köhn and A. Tajti, *J. Chem. Phys.* **127**, 044105 (2007).
- ¹⁷⁶E. F. Kjønstad, R. H. Myhre, T. J. Martínez, and H. Koch, *J. Chem. Phys.* **147**, 164105 (2017).
- ¹⁷⁷S. Thomas, F. Hampe, S. Stopkowicz, and J. Gauss, *Mol. Phys.* **119**, e1968056 (2021).
- ¹⁷⁸M. Thiele and S. Kümmel, *Phys. Rev. Lett.* **112**, 083001 (2014).
- ¹⁷⁹N. T. Maitra, F. Zhang, R. J. Cave, and K. Burke, *J. Chem. Phys.* **120**, 5932 (2004).
- ¹⁸⁰D. Zhang, S. N. Steinmann, and W. Yang, *J. Chem. Phys.* **139**, 154109 (2013).
- ¹⁸¹M. E. Casida, *J. Chem. Phys.* **122**, 054111 (2005).
- ¹⁸²O. V. Gritsenko and E. Jan Baerends, *Phys. Chem. Chem. Phys.* **11**, 4640 (2009).
- ¹⁸³G. Strinati, *Riv. Nuovo Cimento* **11**, 1 (1988).
- ¹⁸⁴D. B. Dar and N. T. Maitra, "Oscillator strengths and excited-state couplings for double excitations in time-dependent density functional theory," [arXiv:2309.08840](https://arxiv.org/abs/2309.08840) [physics.chem-ph] (2023).